

## Simulation Study of the One-Dimensional Burridge-Knopov Model of Earthquakes

Takahiro Mori and Hikaru Kawamura

Department of Earth and Space Science, Faculty of Science, Osaka University, Toyonaka 560-0043, Japan  
(Dated: February 9, 2020)

Spatio-temporal correlations of the one-dimensional spring-block (Burridge-Knopov) model of earthquakes are extensively studied by means of numerical computer simulations. Particular attention is paid to clarifying how the statistical properties of earthquakes depend on the frictional and elastic properties of earthquake faults. It is found that, as the velocity-weakening tendency of the friction force gets weaker, the system tends to be more critical, while, as the velocity-weakening tendency gets stronger, the system tends to be more  $\sigma$ -critical with enhanced features of a characteristic earthquake. The model exhibits several eminent precursory phenomena prior to the large event in its spatio-temporal correlations. Preceding the main shock, the frequency of smaller events is gradually enhanced, whereas, just before the main shock, it is suppressed in a close vicinity of the epicenter of the upcoming event (the Mogi doughnut). The time scale of the onset of the doughnut-like quiescence depends on the extent of the frictional instability. Under certain conditions, preceding the main shock, the apparent  $B$ -value of the magnitude distribution increases significantly. The existence of such distinct precursory phenomena may open a way to the prediction of the time and the position of the upcoming large event.

## I. INTRODUCTION

Earthquake is a stick-slip frictional instability of a fault driven by steady motions of tectonic plates<sup>1,2</sup>. While earthquakes are obviously complex phenomena, certain empirical laws have been known concerning their statistical properties, e.g., the Gutenberg-Richter (GR) law for the magnitude distribution of earthquakes, or the Omori law for the time evolution of the frequency of aftershocks<sup>2</sup>. These laws are basically of statistical nature, becoming eminent only after analyzing large number of events.

Since earthquakes could be regarded as a stick-slip frictional instability of a pre-existing fault, the statistical properties of earthquakes should be governed by the physical law of rock friction<sup>1,2</sup>. One might naturally ask: How the statistical properties of earthquakes depend on the material properties characterizing earthquake faults, e.g., the elastic properties of the crust or the frictional properties of the fault, etc. Answering such questions undoubtedly would give us valuable information in understanding the true nature of earthquakes. Furthermore, the full knowledge of spatio-temporal correlations of earthquakes, particularly those associated with the precursory phenomena of large events, might ultimately open up a door to the statistical prediction of large events.

Meanwhile, a systematic study of the material-parameter dependence of the statistical properties of earthquakes meets serious difficulties, partly because one has to average over large number of events in obtaining the statistically reliable properties of earthquakes, but also because it is difficult to get precise knowledge of, or even to control, various material parameters characterizing real earthquake faults.

In numerical simulation study of earthquakes, on the other hand, these difficulties often become minor ones. In the past, earthquake models of various levels of simplifications have been proposed in geophysics and statistical physics, and their statistical properties have been extensively studied mainly by means of numerical computer simulations. One of the most standard one is the so-called spring-block model originally proposed by Burridge and Knopov (Burridge-Knopov model)<sup>3</sup>. In this model, an earthquake fault is simulated by an assembly of blocks, each of which is connected via the elastic springs to the neighboring blocks and to the moving plate. All blocks are subject to the friction force, the source of the nonlinearity in the model, which eventually realizes an earthquake-like frictional instability. The model contains several parameters representing, e.g., the elastic properties of the crust and the frictional properties of faults.

Carlson, Langer and collaborators performed a pioneering study of the statistical properties of earthquakes<sup>4,5,6,7,8</sup>, based on the spring-block model<sup>3</sup>. These authors paid particular attention to the magnitude distribution of earthquake events, and examined its dependence on the friction parameter characterizing the nonlinear stick-slip dynamics of the model. It was observed that, while smaller events persistently obeyed the GR law, i.e., staying critical or near-critical, larger events exhibited a significant deviation from the GR law, being  $\sigma$ -critical or "characteristic"<sup>4,5,6,7,9</sup>. Shaw, Carlson and Langer studied the same model by examining the spatio-temporal patterns of seismic events preceding large events, observing that the seismic activity accelerates as the large event approaches<sup>10</sup>. Since then, the spring-block model has been extended in several ways, e.g., taking account of the effect of the viscosity<sup>11,12,13</sup>, or modifying the form of the friction force<sup>12,13</sup>.

The study of statistical properties of earthquakes was promoted in early nineties, inspired by the work by P. Bak and collaborators who proposed the concept of "self-organized criticality (SOC)"<sup>14,15</sup>. According to this view, the Earth's

crust is always in the critical state which is self-generated dynamically. The SOC idea gives a natural explanation of the scale-invariant power-law behaviors frequently observed in earthquakes, including the Gutenberg-Richter (GR) law and the Omori law.

The SOC idea was developed mainly on the basis of the cellular-automaton versions of the earthquake model<sup>14,15,16,17,18,19,20,21,22</sup>. The statistical properties of these cellular-automaton models were also studied quite extensively, often interpreted within the SOC framework. These models apparently reproduce several fundamental features of earthquakes such as the GR law, the Omori law of aftershocks, the existence of foreshocks, etc. Although many of these cellular-automaton models were originally introduced to mimic the spring-block model<sup>16,17,18,19,20,21,22</sup>, their statistical properties are not always identical with the original spring-block model. Furthermore, as compared with the spring-block model, the cellular-automaton models are much more simplified so that the model does not have enough room to represent various material properties of the earthquake fault in a physically appealing way. Thus, in the cellular-automaton models, the connection to the material parameters of real earthquake faults is rather obscure.

In the present paper, we perform further extensive investigation of spatio-temporal correlations of earthquakes based on the Burridge-Knopoff (BK) model<sup>3</sup>. Our main goal is to clarify how the statistical properties of earthquakes depend on the frictional and elastic properties of earthquake faults. As compared with the cellular-automaton models, the spring-block model has an advantage that the dependence on the material parameters, including the frictional and elastic properties, are more explicit. We simulate the one-dimensional (1D) version of the BK model. The statistical properties of the model, particularly its spatio-temporal correlations, are studied here by extensive numerical simulations. A preliminary report of the simulation was given in Ref.<sup>23</sup>.

As already mentioned, numerical model simulation is a quite useful tool for our purposes: First, generating huge number of events required to attain the high precision for discussing the statistical properties of earthquakes is easy to achieve in numerical simulations whereas it is often difficult to achieve in real earthquakes especially for larger ones. Second, various material parameters characterizing earthquake faults is extremely difficult to control in real faults, whereas it is easy to control in model simulations.

Although the model studied here, i.e., the 1D BK model is not new and has been studied by previous authors, we simulate the model by more extensive simulations than the previous ones, and investigate the statistical properties of the model through various spatio-temporal correlation functions. As a result, our present simulations have revealed several new interesting features of the model which have hitherto uncovered: These include, i) The doughnut-like quiescence occurring just before the mainshock, ii) a significant change of the  $B$ -value observed prior to the mainshock, and iii) complex behaviors of the recurrence time of large events including the possible twin and unilateral character of large events, etc.

Generally, we have found that as the velocity-weakening tendency of the friction force gets weaker, the system tends to be more critical, while as the velocity-weakening tendency gets stronger, the system tends to be more  $\sigma$ -critical with enhanced features of a characteristic earthquake. Periodic feature of large events is eminent when the friction force exhibits a strong frictional instability, whereas, when the friction force exhibits a weak frictional instability, large events often occur as twin and/or unilateral events. The model turns out to exhibit several eminent precursory phenomena prior to the large event in its spatio-temporal correlations. Preceding the mainshock, the frequency of smaller events is gradually enhanced, whereas, just before the mainshock, it is suppressed in a close vicinity of the epicenter of the upcoming mainshock (the Mogi doughnut<sup>24</sup>). The time scale of the onset of the doughnut-like quiescence depends on the extent of the frictional instability. Under certain conditions, preceding the mainshock, the apparent  $B$ -value of the magnitude distribution increases significantly. This increase of the  $B$ -value is more eminent when the friction force exhibits a strong frictional instability. The existence of such distinct precursory phenomena may open a way to the prediction of the time and the position of the upcoming large event.

The present paper is organized as follows. In §2, we introduce the model and explain some of the details of our numerical simulation. The results of our simulations are presented in §3. Magnitude distribution function, earthquake recurrence-time distribution and various types of spatio-temporal correlation functions of earthquake events are calculated and analyzed. In search of the possible precursory phenomena, particular attention is paid to the time development of the spatial correlation function of earthquake events and of the magnitude distribution function prior to large events. Finally, section 4 is devoted to summary and discussion of our results.

## II. THE MODEL AND THE METHOD

The model we deal with is the one-dimensional Burridge-Knopoff (BK) model<sup>3</sup>. It consists of a 1D array of  $N$  identical blocks, which are mutually connected with the two neighboring blocks via the elastic springs of the elastic constant  $k_c$ , and are also connected to the moving plate via the springs of the elastic constant  $k_p$ . All blocks are subject to the friction force  $\mu$ , which is the only source of nonlinearity in the model. The equation of motion for the

$i$ -th block can be written as

$$m \ddot{U}_i = k_p (\dot{U}_i^0 - \dot{U}_i) + k_c (U_{i+1} - 2U_i + U_{i-1}) - f(\dot{U}_i); \quad (1)$$

where  $t^0$  is the time,  $U_i$  is the displacement of the  $i$ -th block and  $\dot{U}_i^0$  is the loading rate representing the speed of the plate.

In order to make the equation dimensionless, we measure the time  $t^0$  in units of the characteristic frequency  $\omega = \sqrt{k_p/m}$  and the displacement  $U_i$  in units of the length  $L = (0) = k_p / (0)$ ,  $(0)$  being the static friction. Then, the equation of motion can be written in the dimensionless form as

$$\ddot{u}_i = \dot{t} - u_i + l^2 (u_{i+1} - 2u_i + u_{i-1}) - f(\dot{u}_i); \quad (2)$$

where  $t = t^0 \omega$  is the dimensionless time,  $u_i = U_i/L$  is the dimensionless displacement of the  $i$ -th block,  $l = \sqrt{k_c/k_p}$  is the dimensionless stiffness parameter,  $\dot{t} = \dot{U}_i^0/L\omega$  is the dimensionless loading rate, and  $f(\dot{u}_i) = f(\dot{U}_i)/(0)$  is the dimensionless friction force.

In order for the model to exhibit a dynamical instability corresponding to an earthquake, it is essential that the friction force possesses a frictional weakening property, i.e., the friction should become weaker as the block slides. Here, as the form of the friction force, we assume the form used in Ref.<sup>5</sup>, which represents the velocity-weakening friction force;

$$f(\dot{u}_i) = \begin{cases} (1 - \dot{u}_i); & \text{for } \dot{u}_i \leq 0; \\ \frac{1}{1 + 2|\dot{u}_i|}; & \text{for } \dot{u}_i > 0; \end{cases} \quad (3)$$

where its maximum value corresponding to the static friction has been normalized to unity. As noted above, this normalization condition  $f(\dot{u}_i = 0) = 1$  has been utilized to set the length unit  $L$ . The back-slip is inhibited by imposing an infinitely large friction for  $\dot{u}_i < 0$ , i.e.,  $f(\dot{u}_i < 0) = \infty$ .

The friction force is characterized by the two parameters,  $\alpha$  and  $\beta$ . The former,  $\alpha$ , introduced in Ref.<sup>5</sup> as a technical device, represents an instantaneous drop of the friction force at the onset of the slip, while the latter,  $\beta$ , represents the rate of the friction force getting weaker on increasing the sliding velocity. In the present simulation, we regard  $\alpha$  to be small, and  $\beta = 0.01$ .

We note that there have been several other proposals for the law of rock friction, e.g., the slip-weakening friction force<sup>1,2,25,26</sup> or the rate- and state-dependent friction force<sup>1,2,27,28</sup>. We assume here the simplest version of the velocity-weakening friction force given above.

Following Ref.<sup>5</sup>, we also assume the loading rate  $\dot{t}$  to be infinitesimally small, and put  $\dot{t} = 0$  during an earthquake event, a very good approximation for real faults. Taking this limit ensures that the interval time during successive earthquake events can be measured in units of  $t^0$  irrespective of particular values of  $\dot{t}$ . Taking the  $\dot{t} \rightarrow 0$  limit also ensures that, during an ongoing event, no other event takes place at a distant place, independently of this ongoing event.

Then, the model possesses one more parameter, a dimensionless stiffness parameter  $l$ , which describes the elastic property of the crust.

We solve the equation of motion (2) by using the Runge-Kutta method of the fourth order. The width of the time discretization  $\Delta t$  is taken to be  $\Delta t = 10^{-6}$ . We have checked that the statistical properties given below are unchanged even if we take the smaller  $\Delta t$ . Total number of  $10^7$  events are generated in each run, which are used to perform various averagings. In calculating the observables, initial  $10^4$  events are discarded as transients.

In order to eliminate the possible finite-size effects, the total number of blocks are taken to be large, typically  $N = 800$ , with periodic boundary conditions. In the case of typical parameter values, say,  $l = 3$  and  $\beta = 0.01$ , even the largest event in our simulations involves the number of blocks less than  $N = 800$ .

We study the properties of the model with varying the frictional parameter  $\beta$  and the elastic parameter  $l$ . Particular attention is paid to the dependence on the parameter  $\beta$ , since the parameter  $l$ , which represents the extent of the frictional weakening, turns out to affect the result most significantly.

### III. THE RESULTS

In this section, we show the results of our numerical simulations for several observables, i.e., (A) magnitude distribution of events, (B) mean displacement of blocks at each large event, (C) local recurrence-time distribution of large events, (D) global recurrence-time distribution of large events, (E) magnitude correlations between successive large events, (F) time correlations of events associated with the mainshock, (G) spatial correlations of events before the mainshock, (H) spatial correlations of events after the mainshock, (I) time-resolved magnitude distribution of events before and after the mainshock, etc. Below, we show these results consecutively.

### A . M agnitude distribution

In Fig.1 we show the magnitude distribution  $R(\mu)$  of earthquake events, where  $R(\mu)$  represents the rate of events with their magnitudes in the range  $[\mu; \mu + d]$ . The parameter  $\alpha$  is varied in the range 0.25 to 10, while the parameters  $l$  in the range 2 to 4.

The magnitude of an event,  $\mu$ , is defined as the logarithm of the moment  $M_0$ , i.e.,

$$\mu = \ln M_0; \quad M_0 = \sum_i u_i; \quad (4)$$

where  $u_i$  is the total displacement of the  $i$ -th block during a given event and the sum is taken over all blocks involved in the event<sup>5</sup>.

As can be seen from Fig.1, the form of the calculated  $R(\mu)$  depends on the  $\alpha$ -value considerably. The data for  $\alpha = 1$  lie on a straight line fairly well, apparently satisfying the GR law. The values of the exponent  $B$  describing the power-law behavior,  $R(\mu) \propto 10^{-B\mu}$ , is estimated to be  $B \approx 0.50$ .

As can be seen from Fig.1 (a), the data for larger  $\alpha$ , i.e., the ones for  $\alpha \geq 2$  deviate from the GR law at larger magnitudes, exhibiting a pronounced peak structure, while the power-law feature still remains for smaller magnitudes. These features of the magnitude distribution are consistent with the earlier observation of Carlson and Langer<sup>4,5</sup>. It means that, while smaller events exhibit self-similar critical properties, larger events tend to exhibit non-critical or characteristic properties, much more so as the velocity-weakening tendency of the friction is increased.

The observed peak structure gives us a criterion to distinguish large and small events. Below, we regard events with their magnitudes greater than  $\mu_c = 3$  as large events,  $\mu_c = 3$  being close to the peak position of the magnitude distribution of Fig.1. In an earthquake with  $\alpha = 3$ , the mean number of moving blocks are about 76 ( $l = 1$ ) and 60 ( $l = 2; 3$ ).

By contrast, as can be seen from Fig.1 (b), the data for smaller  $\alpha < 1$  exhibit considerably different behaviors from those for  $\alpha > 1$ . Large events are suppressed here. For  $\alpha = 0.25$ , in particular, all events consist almost exclusively of small events only. This result might be consistent with the earlier observation of Ref.<sup>4</sup>, which suggested that the smaller value of  $\alpha < 1$  tended to cause a creeping-like behavior without a large event. Since we are mostly interested in large seismic events in the present paper, we concentrate in the following on the parameter range  $\alpha \geq 1$ . We mainly study the cases  $\alpha = 1; 2$  and 3 since further increase of  $\alpha > 3$  does not change the results qualitatively, as can be seen from Fig.1 (a).

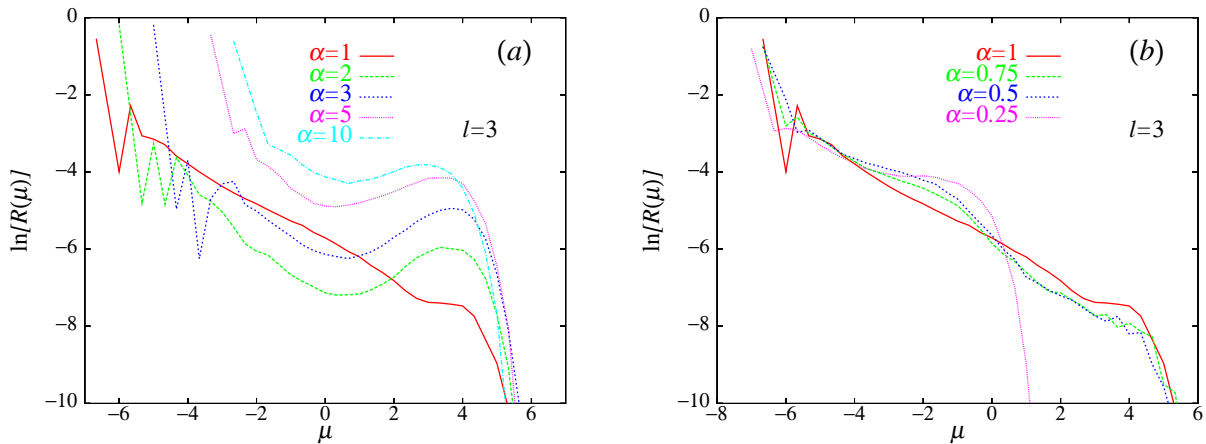


FIG. 1: Magnitude distribution of earthquake events for various values of  $\alpha$ ; (a) for larger  $\alpha = 1; 2; 3; 5$  and 10, and (b) for smaller  $\alpha = 0.25; 0.5; 0.75$  and 1. The parameter  $l$  is fixed to be  $l = 3$ .

In Fig.2, we show the magnitude distribution  $R(\mu)$  with varying the values of the stiffness parameter  $l$  for the case of  $\alpha = 1$  (Fig.2 (a)) and  $\alpha = 2$  (Fig.2 (b)). In either case, the form of the magnitude distribution  $R(\mu)$  does not change qualitatively with  $l$ , although larger  $l$  tends to make the largest possible event even larger. This tendency is intuitively easy to understand, since as the system becomes stiffer the stress release would be made via a huge event involving larger number of blocks. In the case of  $\alpha = 1$ , the power-law feature persists for any  $l$ , the associated  $B$ -value being  $B \approx 0.56$  ( $l = 2$ ) and  $B \approx 0.46$  ( $l = 4$ ).

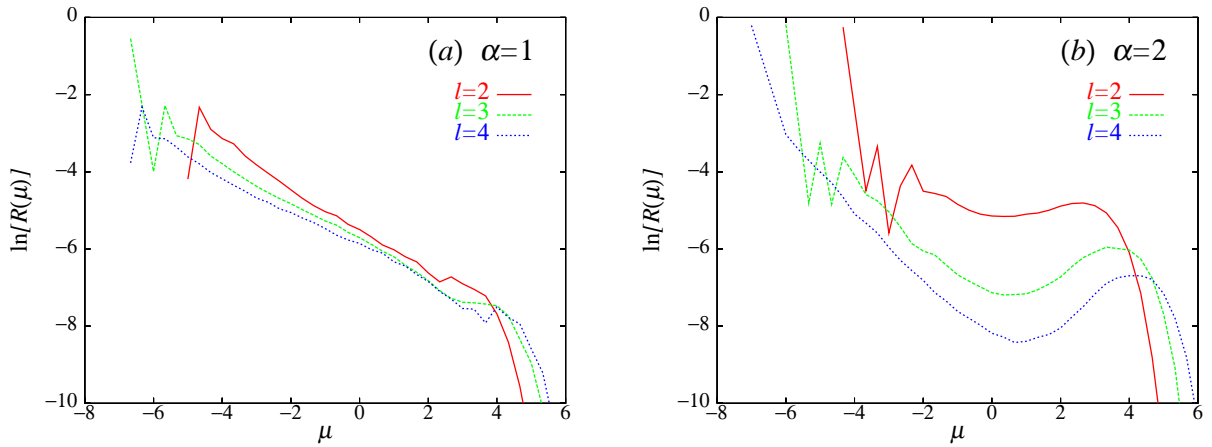


FIG. 2: M magnitude distribution of earthquake events for various values of  $l$ ; (a) for  $\alpha=1$  and (b) for  $\alpha=2$ .

### B. Mean displacement of blocks in large events

In order to clarify how the seismic rupture proceeds in each large event, we show in Fig.3 the mean displacement of a block which is apart from the epicenter of the event by distance  $r$ . The average is made over all events with their magnitudes in the range  $4 < \mu < 5$ . In the figure, we always take the  $r > 0$  side to be the side in which the rupture propagates farther, and the  $r < 0$  side to be the side in which the rupture propagates less,  $r = 0$  being the epicenter of the event. From Fig.3, one can see the following features: (i) The block displacement is not maximum at the epicenter, whereas the maximum displacement occurs somewhat apart from the epicenter. The block which triggers the large event does not move much itself. This tendency becomes more pronounced for smaller  $\alpha$ . The ratio of the mean displacement at the epicenter (the block at  $r = 0$ ) to the maximum mean displacement is 0.054, 0.70 and 0.74 for  $\alpha = 1; 2$  and  $3$ , respectively. (ii) The asymmetry of the curves in Fig.3 with respect to  $r = 0$  becomes more pronounced for smaller  $\alpha$ . In the case of  $\alpha = 1$ , in particular, the rupture propagates almost in one direction only, and the event occurs as a "unilateral earthquake". In other words, for  $\alpha = 1$ , the epicenter of large events tend to be located near the edge of the rupture zone. This can be confirmed more quantitatively by calculating the "eccentricity" of the epicenter  $e = R_e/R$ , which is defined by the ratio of the mean distance between the epicenter and the center of mass of the rupture zone,  $R_e$ , to the mean radius of the rupture zone,  $R$ . Then, we have found  $e = 0.88, 0.52$  and  $0.53$  for the cases  $\alpha = 1, 2$  and  $3$ , respectively. The occurrence of unilateral earthquakes for smaller  $\alpha$  may naturally be understood if one notes that the relative weakness of the stick-slip instability prevents the initiated rupture from propagating far into both directions.

### C. Local recurrence-time distribution

A question of general interest may be how large earthquakes repeat in time, do they occur near periodically or irregularly? One may ask this question either locally, i.e., for a given finite area on the fault, or globally, i.e., for an entire fault system. The picture of characteristic earthquake presumes the existence of a characteristic recurrence time. In that case, the distribution of the recurrence time of large earthquakes,  $T$ , is expected to exhibit a peak structure at such a characteristic time scale. If the SOC concept applies to large earthquakes, on the other hand, such a peak structure would not show up.

In Fig.4, we show the distribution of the recurrence time  $T$  of large earthquakes with  $\alpha_c = 3$ , measured locally. In the insets, the same data including the tail part are re-plotted on a semi-logarithmic scale. In defining the recurrence time locally, the subsequent large event is counted when a large event occurs with its epicenter in the region within 30 blocks from the epicenter of the previous large event. The mean recurrence time  $T$  is then estimated to be  $T = 1.47, 1.12$ , and  $1.13$  for  $\alpha = 1, 2$  and  $3$ , respectively.

The local recurrence-time distribution shown in Fig.4 has the following two noticeable features. (i) The tail of the distribution is exponential at longer  $T > T_c$  for all values of  $\alpha$ . Such an exponential tail of the distribution has also been reported for real faults<sup>29</sup>. (ii) The form of the distribution at shorter  $T < T_c$  is non-exponential, and largely differs between for  $\alpha = 1$  and for  $\alpha = 2$  and  $3$ . For  $\alpha = 2$  and  $3$ , the distribution has an eminent peak at around

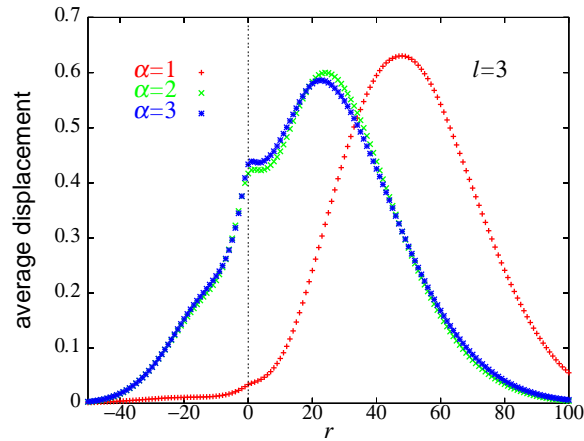


FIG. 3: Mean displacement of blocks in large events with their magnitudes in the range  $3.5 \leq M \leq 5$  plotted versus the distance of a block from the epicenter of the event. The  $r > 0$  side is taken to be the side in which the rupture propagates farther, and the  $r < 0$  side to be the side in which the rupture propagates less,  $r = 0$  being the epicenter of the event. The parameter  $\alpha$  is  $\alpha = 1; 2$  and  $3$ .

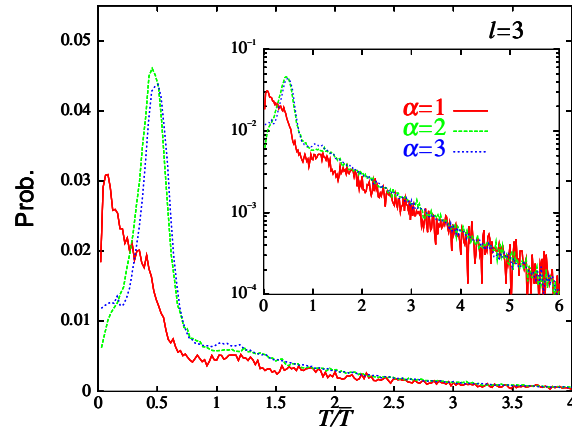


FIG. 4: The local recurrence-time distribution of large events with their magnitudes greater than  $M_c = 3$  for various values of  $\alpha$ . The parameter  $l$  is fixed to be  $l = 3$ . The recurrence time  $T$  is normalized by its mean  $T$ , which are  $T = 1.47, 1.12$ , and  $1.13$  for  $\alpha = 1, 2$  and  $3$ , respectively. The insets represent the semi-logarithmic plots including the tail part of the distribution.

$T \approx 0.5$ , not far from the mean recurrence time. This means the existence of a characteristic recurrence time, suggesting the near-periodic recurrence of large events. Indeed, such a near-periodic recurrence of large events was reported for several real faults<sup>2,30</sup>.

For  $\alpha = 1$ , by contrast, the peak located close to the mean  $T$  is hardly discernible. Instead, the distribution has a pronounced peak at a shorter time  $T \approx 0.10$ , just after the previous large event. In other words, large events for  $\alpha = 1$  tend to occur as "twins". This has also been confirmed by our analysis of the time record of large events.

As was noticed in Fig.3, a large event for the case of  $\alpha = 1$  often occurs as a "unilateral earthquake" where the rupture propagates only in one direction, hardly propagating in the other direction. When a large earthquake occurs in the form of such a unilateral earthquake, further loading due to the plate motion tends to trigger the subsequent large event in the opposite direction, causing a twin-like event. This naturally explains the small- $T$  peak observed in Fig.4 for  $\alpha = 1$ .

The distribution functions for  $\alpha = 2$  and  $3$  can be well fitted by the sum of the exponential representing the tail part and the Gaussian representing the peak part,

$$C_1 \exp\left[-\frac{1}{2}\left(\frac{T-T_1}{T}\right)^2\right] + C_2 \exp\left[-\frac{T}{T_2}\right]; \quad (5)$$

where  $T_1 \approx 0.51$ ,  $T \approx 0.12$ ,  $T_2 \approx 1.40$  for  $\alpha = 2$ , and  $T_1 \approx 0.57$ ,  $T \approx 0.12$ ,  $T_2 \approx 1.45$  for  $\alpha = 3$ , respectively. For  $\alpha = 1$ , by contrast, the short-time part cannot be fitted by the Gaussian, although the tail part of the distribution can be well fitted by the exponential with  $T_2 \approx 1.98$ .

In Fig.5, the recurrence-time distribution of large events is shown for the cases of  $\alpha = 1$  (a) and  $\alpha = 2$  (b), with varying the magnitude threshold as  $\mu_c = 2, 3$  and 4. As can be seen from Fig.5(a), the form of the distribution for  $\alpha = 1$  largely changes with the threshold value  $\mu_c$ . Interestingly, in the case of  $\mu_c = 4$ , the distribution has two distinct peaks, one corresponding to the twin-like event and the other to the near-periodic event. Thus, even in the case of  $\alpha = 1$  where the critical features are apparently dominant for smaller thresholds  $\mu_c = 2$  and 3, features of a characteristic earthquake becomes increasingly eminent when one looks at very large events.

As can be seen from Fig.5(b), on the other hand, the form of the recurrence-time distribution for  $\alpha = 2$  is rather insensitive to the threshold value  $\mu_c$ , always keeping an pronounced peak structure. The peak position varies with  $\mu_c$  considerably, however, reflecting the change of the mean recurrence time  $T$  with  $\mu_c$ , i.e.,  $T \approx 0.76$  ( $\mu_c = 2$ ),  $T \approx 1.12$  ( $\mu_c = 3$ ) and  $T \approx 2.58$  ( $\mu_c = 4$ ).

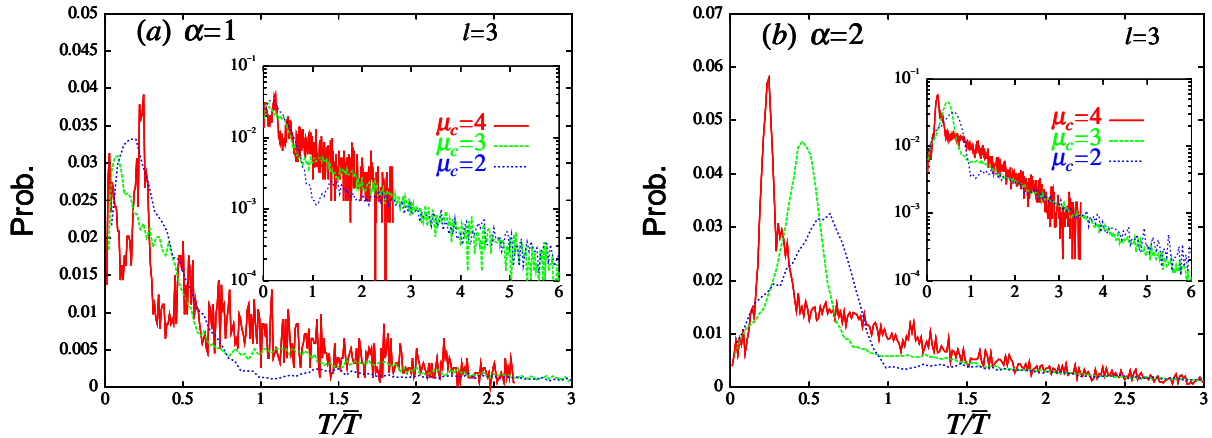


FIG. 5: The local recurrence-time distribution of large events for various values of the magnitude threshold  $\mu_c$  for the cases of  $\alpha = 1$  (a), and  $\alpha = 2$  (b). The recurrence time  $T$  is normalized by its mean  $\bar{T}$ , which are  $\bar{T} = 0.76, 1.47$ , and  $3.42$  for  $\mu_c = 2, 3$  and 4 in the case of  $\alpha = 1$ , while  $\bar{T} = 0.76, 1.12$ , and  $2.58$  for  $\mu_c = 2, 3$  and 4 in the case of  $\alpha = 2$ , respectively. The insets represent the semi-logarithmic plots including the tail part of the distribution.

In Fig.6, we show the local recurrence-time distribution of large events (with the threshold value  $\mu_c = 3$  here) for various values of the parameter  $l$ , for the cases of  $\alpha = 1$  (a) and  $\alpha = 2$  (b). As can be seen from the figures, qualitative features of the recurrence-time distribution are not very sensitive to the  $l$ -value, although periodic features tend to be enhanced for larger  $l$ .

#### D. Global recurrence-time distribution

In Fig.7, we show the global recurrence-time distribution of large events with  $\mu_c = 3$ , i.e., the one for an entire fault system with  $N = 800$  for various values of  $\alpha$ . The parameter  $l$  is fixed to be  $l = 3$ . As can clearly be seen from the figure, the form of the distribution takes a different form from the local one. The peak structure seen in the local distribution no longer exists here. Furthermore, the form of the distribution tail at larger  $T$  is no longer a simple exponential, faster than exponential: See a curvature of the data in the inset of Fig.7. These features of the global recurrence-time distribution turn out to be rather robust against the change of the  $l$ -value.

The present observation that the local and the global recurrence-time distributions exhibit mutually different behaviors means that the form of the distribution depends on the length scale of measurements, as well as on the  $\alpha$ -value. Such scale-dependent features of the recurrence-time distribution of the BK model is in apparent contrast with the scale-invariant features of the recurrence-time distributions recently reported for some of real faults<sup>29,31</sup>.

#### E. Magnitude correlations between successive large events

In the previous subsections, we studied the recurrence time, i.e., the time elapsed between two successive large events. In this subsection, we study the correlation between the magnitudes of the two successive large events. There

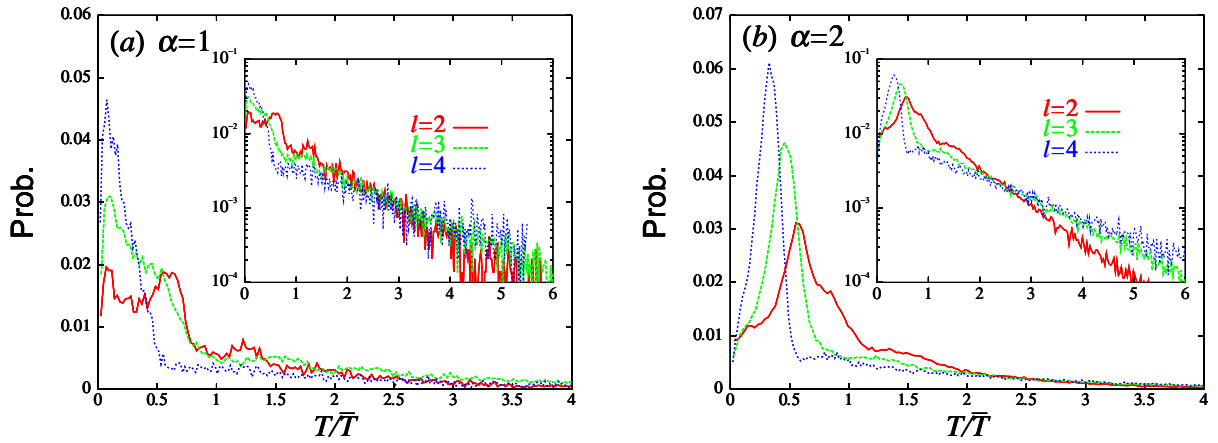


FIG. 6: The local recurrence-time distribution of large events with their magnitudes greater than  $m_c = 3$  for various values of  $l$ , for the cases of  $\alpha = 1$  (a) and  $\alpha = 2$  (b). The recurrence time  $T$  is normalized by its mean  $\bar{T}$ , which are  $\bar{T} = 1.30, 1.47$ , and  $1.64$  for  $l = 2, 3$  and  $4$  in the case of  $\alpha = 1$ , while  $\bar{T} = 1.03, 1.12$ , and  $1.47$  for  $l = 2, 3$  and  $4$  in the case of  $\alpha = 2$ , respectively. The insets represent the semi-logarithmic plots including the tail part of the distribution.

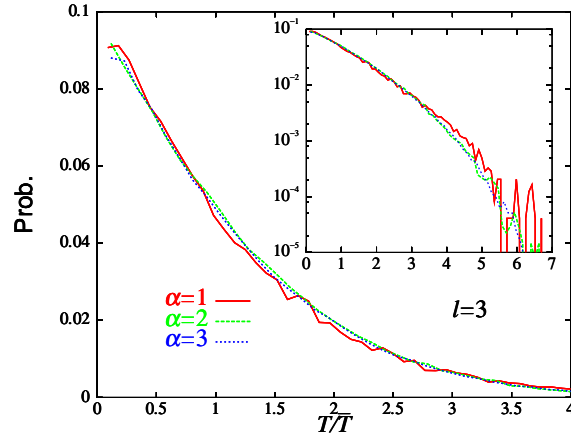


FIG. 7: The global recurrence-time distribution of large events with their magnitudes greater than  $m_c = 3$  for various values of  $\alpha$ . The recurrence time  $T$  is normalized by its mean  $\bar{T}$ , which are  $\bar{T} = 0.011, 0.086$  and  $0.087$  for  $\alpha = 1, 2$  and  $3$ , respectively. The insets represent the semi-logarithmic plots including the tail part of the distribution.

are two common views concerning the magnitudes of the two successive large events. One is that there is no correlation between the magnitudes of the two successive large events. The other is that there is an anti-correlation between the magnitudes of the two successive large events, i.e., when the first event happens to be not so large, then the next event tends to be larger, and vice versa. This tendency might naturally be expected, since, when the first event is only moderate, the stress accumulated in the region might not fully be released, which might make the next event even larger.

In Figs.8 (a)–(c), we show in the cases of  $\alpha = 1, 2$  and  $3$  the magnitude distribution of large events with  $m_c = 3$  for various values of the magnitude of the large event preceding this event. The parameter  $l$  is taken to be  $l = 3$ . As in Figs.4–6, the successive large event is identified when an event of its magnitude  $> m_c = 3$  occurs with its epicenter lying in the region less than  $30$  blocks from the epicenter of the preceding large event.

As can be seen from Fig.8 (a), a correlation is hardly appreciable between the magnitudes of the successive large events in the case of  $\alpha = 1$ . In the cases of  $\alpha = 2$  and  $3$ , by contrast, there is a weak anti-correlation between the magnitudes of the two successive events, i.e., the next event tends to be larger when the first event is moderate, and vice versa. Hence, there seems to be a tendency that the larger  $\alpha$ -value induces an anti-correlation between the magnitudes of the two successive large events.

In Figs.9 (a) and (b), we show the magnitude distribution of large events for various values of the magnitude of the

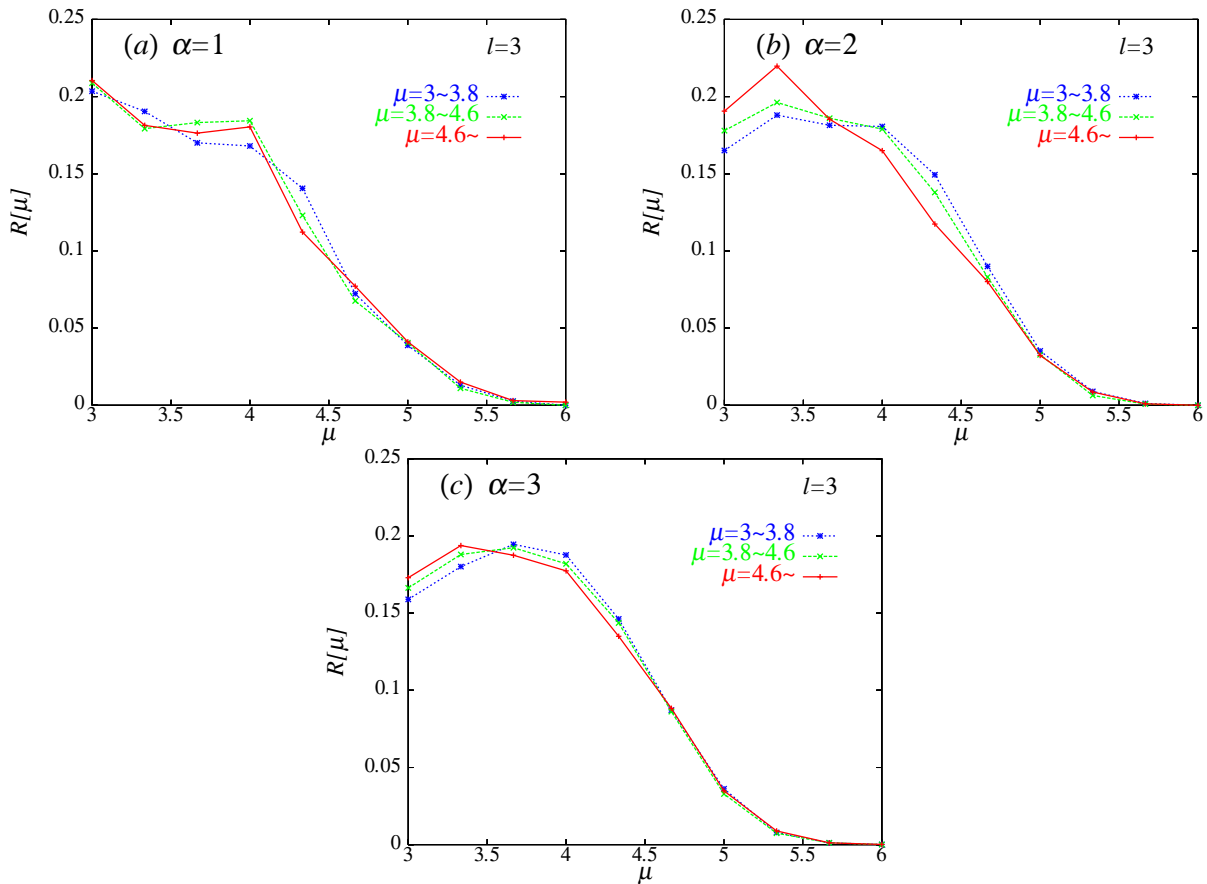


FIG. 8: The magnitude distribution of large events with their magnitudes greater than  $\mu_c = 3$  plotted with varying the magnitudes of the last large event preceding this event. The parameter  $\alpha$  is  $\alpha = 1$  (a),  $\alpha = 2$  (b), and  $\alpha = 3$  (c), where  $l$  is fixed to be  $l = 3$ .

large event preceding this event, for the cases of  $l = 2$  (a) and  $l = 4$  (b), with  $\mu_c = 2$ . As can be seen from the figures, there is a tendency that the larger  $l$ -value induces an anti-correlation between the magnitudes of the two successive large events.

If one combines the observation here with those of the previous subsections, one may conclude that there is no correlation between the magnitudes of the two successive events when an earthquake is "critical" (as it should be), whereas there appears an anti-correlation between the magnitudes of the two successive events when an earthquake is "characteristic".

#### F. Time correlation of events associated with the mainshock

In Fig.10 (a), we show the time correlation function between large events and events of arbitrary sizes (dominated in number by small events) for various values of the parameter  $\alpha$ . More precisely, we plot the mean number of events of arbitrary sizes occurring within 30 blocks from the epicenter of the mainshock before ( $t < 0$ ) and after ( $t > 0$ ) the mainshock, where the occurrence of the mainshock is taken to be the origin of the time  $t = 0$ . The average is taken over all large events of their magnitudes with  $\mu_c = 3$ . Note that, by this way of event counting, when more than one large event occurs successively close in time, the same event might be counted more than once in the time correlation function at distinct times  $t$ , each associated with distinct large events. The number of events are counted here with the time bin of  $\Delta t = 0.02$ .

As can be seen from Fig.10 (a), after the mainshock, the seismic activity stays at lower level for some period, which corresponds to the calm period or quiescence. In the cases of  $\alpha = 2$  and  $3$ , this calm period continues during about half of the recurrence time of large events. After this calm period, the seismicity is gradually activated, eventually leading to the next large event, which manifests itself in the peak of the time correlation function at around  $t' = T$ .

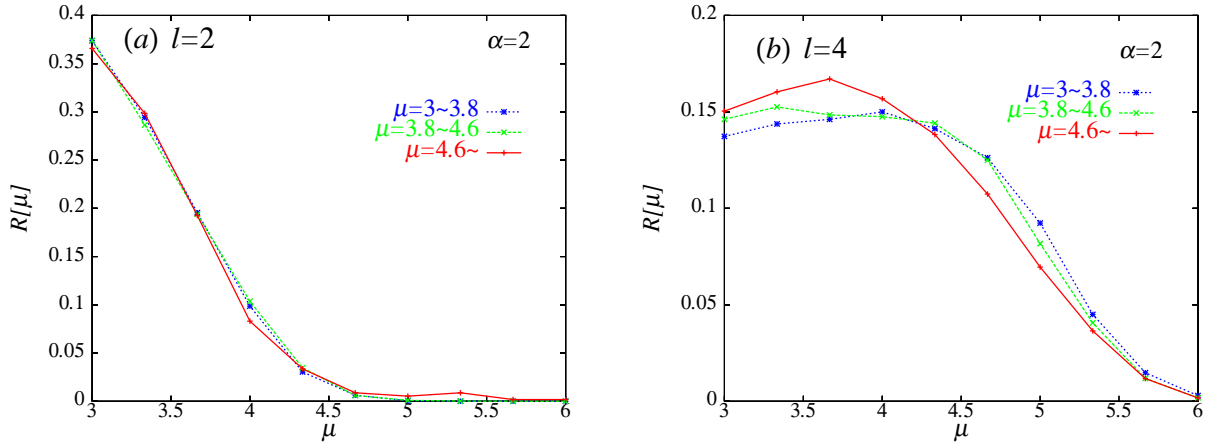


FIG. 9: The magnitude distribution of large events with their magnitudes greater than  $\mu_c = 3$  plotted with varying the magnitudes of the last large event preceding this event. The parameter  $l$  is  $l = 2$  (a) and  $l = 4$  (b), where  $\alpha$  is fixed to be  $\alpha = 2$ .

Thus, for the cases of  $\alpha = 2$  and  $3$ , the interval period between the two large events can be divided into two halves: The former half is the calm period where the seismic activity stays at lower level, while the latter half is the active period where the seismic activity attains higher level.

In the case of  $\alpha = 1$ , by contrast, the calm period after the mainshock is very short, and the active seismicity resumes soon after the mainshock. This immediate seismic activation after the mainshock in the case of  $\alpha = 1$  may be understood as associated with the next large event which tends to occur immediately after the large event as a "two-block"-like event: See Fig. 4.

Before the mainshock ( $t < 0$ ), a remarkable acceleration of seismic activity occurs irrespective of the  $\alpha$ -value. Hence, the existence of the active period preceding the mainshock appears to be a general property of the BK model.

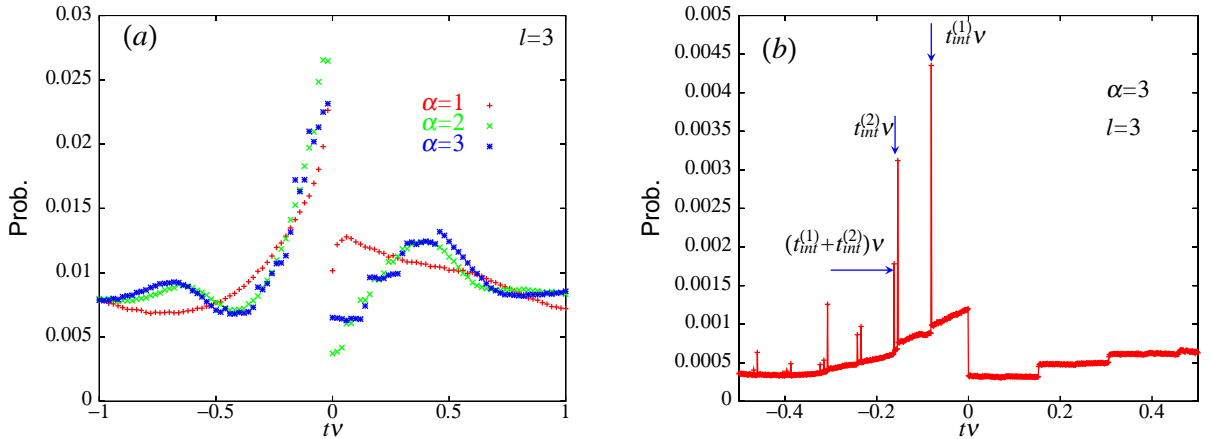


FIG. 10: The time correlation function between large events occurring at time  $t = 0$  and events of arbitrary sizes (dominated in number by small events) occurring at time  $t$  for various values of  $\alpha$ . Events of arbitrary sizes occurring within 30 blocks from the epicenter of the large event are counted. The negative time  $t < 0$  represents the time before the mainshock, while the positive time  $t > 0$  represents the time after the mainshock. The average is taken over all large events with its magnitude  $\mu > \mu_c = 3$ . In (a), the number of events are counted with the time bin of  $\Delta t = 0.02$ , while in (b), it is counted with the higher time resolution of  $\Delta t = 0.001$ .

Closer inspection of Fig. 10 (a) reveals that the calculated time-correlation function exhibits irregular structures, particularly in the case of  $\alpha = 3$ . Thus, we show in Fig. 10 (b) the time-correlation function for  $\alpha = 3$  with higher time resolution than in Fig. 10 (a), i.e., the number of events are counted here with the smaller time bin of  $\Delta t = 0.001$ . Now, it can clearly be seen from Fig. 10 (b) that several "spikes" appear in the time correlation function. It turns out that all these spikes consist almost exclusively of one-block events. Furthermore, all the interval times between these

spike-like events and the mainshock at  $t = 0$  are given by the linear combination of the two elementary interval times  $t_{\text{int}}^{(1)}$  and  $t_{\text{int}}^{(2)}$  as  $n_1 t_{\text{int}}^{(1)} + n_2 t_{\text{int}}^{(2)}$  ( $n_1$  and  $n_2$  integers): See the arrows in Fig.10 (b).

In the present model, one can see that the block motions in all possible one-block events are exactly the same when measured from their stopping sites irrespective of the positions of the neighboring blocks so long as only one block is involved in the event. This is an immediate consequence of the equation of motion of the model (2). Now, suppose that there occurs a one-block event at the block  $i$  while the same block  $i$  triggers the next event some time after this one-block event, i.e., the block  $i$  happens to be an epicenter of the next event which may be either one-block event or many-blocks event. When the two neighboring blocks  $i-1$  are kept stopped during this time period, the interval time between the one-block event and the next event triggered by the block  $i$  is uniquely determined for all possible one-block events, which is equal to  $t_{\text{int}}^{(2)}$  given above. On the other hand, when one of the neighboring blocks, i.e., either the one at  $i-1$  or at  $i+1$  exhibits a one-block event during this time period, the interval time is again uniquely determined for all possible one-block events, and is equal to  $t_{\text{int}}^{(1)}$  given above. These two interval times  $t_{\text{int}}^{(1)}$  and  $t_{\text{int}}^{(2)}$ , i.e., the interval times between the one-block event and the next event of arbitrary sizes triggered by the same block, are easily calculable from the equation of the motion (2) as a function of the parameters  $\alpha$  and  $l$ . The results are shown in Fig.11. Both  $t_{\text{int}}^{(1)}$  and  $t_{\text{int}}^{(2)}$  increase with increasing  $\alpha$ . In fact, the interval times between the spikes observed in Fig.10 (b) can be well described by the linear combination of the calculated  $t_{\text{int}}^{(1)}$  and  $t_{\text{int}}^{(2)}$ : In the case of  $\alpha = 3$  and  $l = 3$  corresponding to Fig.10 (b),  $t_{\text{int}}^{(1)}$  and  $t_{\text{int}}^{(2)}$  are calculated to be  $t_{\text{int}}^{(1)} = 0.081$  and  $t_{\text{int}}^{(2)} = 0.154$ .

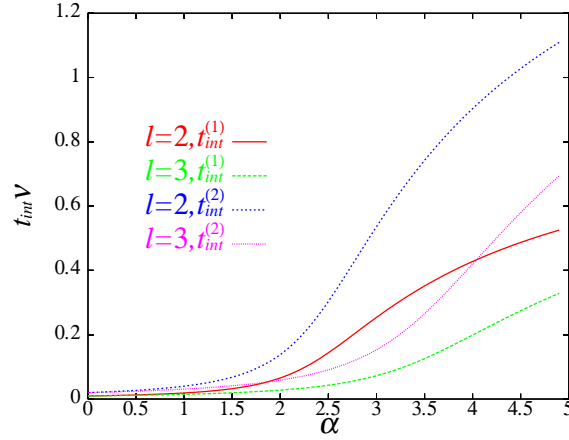


FIG. 11: The two elementary interval times  $t_{\text{int}}^{(1)}$  and  $t_{\text{int}}^{(2)}$ , i.e., the interval times between the one-block event and the next event of arbitrary sizes triggered by the same block, calculated from the equation of motion as a function of the parameters  $\alpha$  and  $l$ . For more detailed definition, see the text.

Although the existence of such characteristic interval times associated with the one-block event,  $t_{\text{int}}^{(1)}$  and  $t_{\text{int}}^{(2)}$ , is an inevitable attribute of the present model, it is not clear at the present stage whether this property of the BK model has a counterpart in real earthquakes in some way or other. Further studies are required to clarify this point.

### G. Spatial correlations of events before the mainshock

In this subsection, we examine the time-development of spatial correlations of events preceding the mainshock. Fig.11 represents the spatial correlation function between the mainshock and the preceding events of arbitrary sizes (dominated in number by smaller events) for several time periods before the mainshock, for the cases of  $\alpha = 1$  (a),  $\alpha = 2$  (b) and  $\alpha = 3$  (c): It represents the conditional probability that, provided that a large event with  $\alpha > \alpha_c = 3$  occurs at a time  $t_0$  and at a spatial point  $r_0$ , an event of arbitrary sizes occurs at a time  $t_0 - t$  and at a spatial point  $r_0 - r$ . The calculated spatial correlation functions for the cases of  $\alpha = 1; 2$  and  $3$  are shown as a function of  $r$ .

As can be seen from Fig.12, preceding the mainshock, there is a tendency of the frequency of smaller events to be enhanced at and around the epicenter of the upcoming mainshock irrespective of the  $\alpha$ -value<sup>10</sup>. For small enough  $t$ , such a cluster of smaller events correlated with the large event may be regarded as foreshocks. Such an enhancement of smaller events preceding the large event was observed by Shaw et al<sup>10</sup>. Interestingly, however, as the mainshock becomes imminent, the frequency of smaller events is suppressed in a close vicinity of the epicenter of the upcoming mainshock, though it continues to be enhanced in the surroundings. For real earthquake faults, such a quiescence

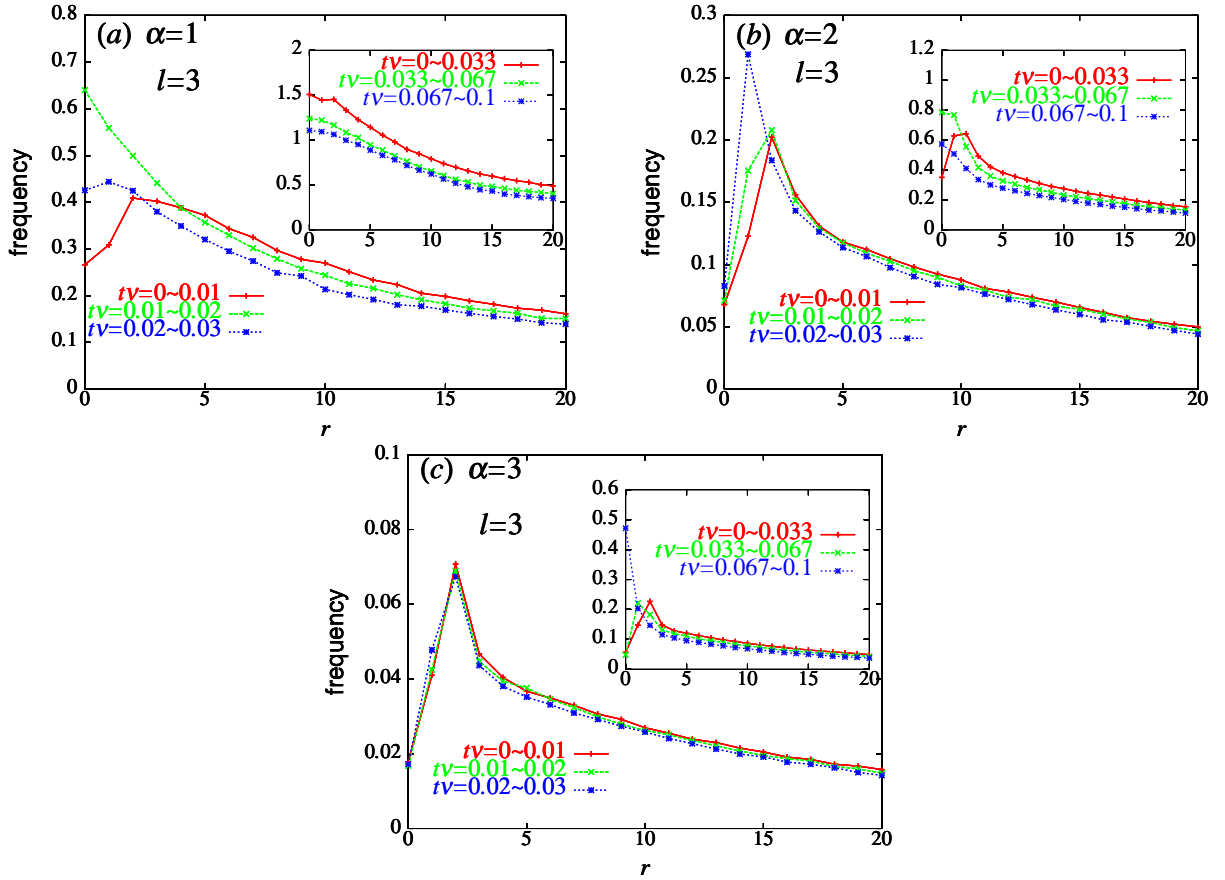


FIG. 12: Event frequency preceding the large event with  $v_c = 3$  plotted versus  $r$ , the distance from the epicenter of the upcoming mainshock, for several time periods before the mainshock. The parameter  $\alpha$  is 1 (a), 2 (b) and 3 (c). The insets represent similar plots with larger time intervals.

phenomenon has been discussed as the "doughnut"<sup>2,24</sup>. The present observation contrasts with the earlier work of Carlson, who claimed that the 1D BK model did not exhibit such a doughnut-like quiescence<sup>6</sup>. We note that the quiescence observed here occurs only in a close vicinity of the epicenter of the mainshock, within one or two blocks from the epicenter, and only at a time close to the mainshock. The time scale for the appearance of the doughnut-like quiescence depends on the  $\alpha$ -value. Namely, the time scale of the onset of the doughnut-like quiescence tends to be shorter for smaller  $\alpha$ , as can be seen from Figs.12 (a)-(c).

The doughnut-like quiescence observed here is closely related to the characteristic interval time scales associated with the single-block event,  $t_{\text{int}}^{(1)}$  and  $t_{\text{int}}^{(2)}$ , discussed in the previous subsection. Namely, the time scale of the onset of the doughnut-like quiescence is basically determined by  $t_{\text{int}}^{(1)}$  and  $t_{\text{int}}^{(2)}$ . Indeed, the time scale of the onset of the doughnut-like quiescence turns out to be well described by the interval times calculated in Fig.11 including its dependence on the parameters  $\alpha$  and  $l$ . For example, in the case of  $\alpha = 1$  and  $l = 3$  corresponding to Fig.12 (a), the interval time  $t_{\text{int}}^{(1)}$  is estimated to be  $t_{\text{int}}^{(1)} = 0.016$ , which gives a reasonable measure of the onset time scale of the doughnut-like quiescence observed in Fig.12 (a).

In the present model, the size of the "hole" of the doughnut-like quiescence as well as its onset time scale have no correlation with the magnitude of the upcoming event, as has been expected from its interpretation in terms of  $t_{\text{int}}^{(1)}$  and  $t_{\text{int}}^{(2)}$ . In other words, the doughnut-like quiescence is not peculiar to large events in the present model. This means that, by monitoring the onset of the "hole" in the seismic pattern, one can certainly deduce the time and the position of the upcoming event, but unfortunately, cannot tell about its magnitude. Yet, one might get some information about the magnitude of the upcoming event, not from the size and the onset time of the "hole", but from the size of the "ring" surrounding the "hole". Thus, we show in Figs.13 the spatial correlation functions before the mainshock in the time range  $0 \leq t \leq 0.001$  for the case of  $\alpha = 2$ , with varying the magnitude range of the upcoming event. In the figure, the direction in which the rupture propagates farther in the upcoming event is always taken to be the positive

direction  $r > 0$ , whereas the direction in which the rupture propagates less is taken to be the negative direction  $r < 0$ . As can be seen from the figure, although the size of the "hole" around the origin  $r = 0$  has no correlation with the magnitude of the upcoming event as mentioned above, the size of the region of the active seismicity surrounding this "hole" is well correlated with the size and the direction of the rupture of the upcoming event. This coincidence might enable one to deduce the position and the size of the upcoming event by monitoring the pattern of foreshocks, although it is still difficult to give a pinpoint prediction of the time of the upcoming mainshock.

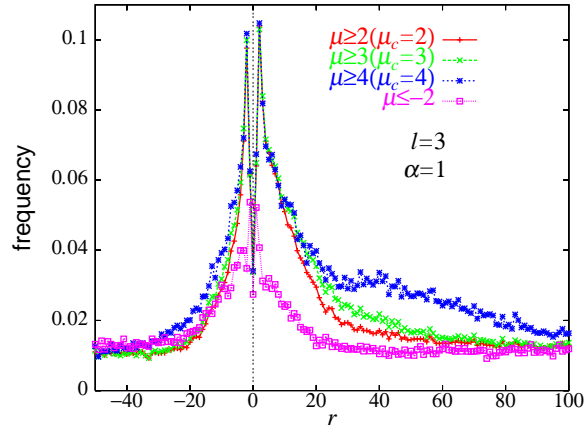


FIG. 13: Event frequency preceding the events of various magnitude range plotted versus  $r$ , the distance from the epicenter of the upcoming mainshock. The curves correspond to the large events with  $\mu > \mu_c = 2; 3$  and 4, and to the smaller events with  $\mu < -2$ . The direction in which the rupture propagates farther in the upcoming mainshock is always taken to be the positive direction  $r > 0$ , whereas the direction in which the rupture propagates less is taken to be the negative direction  $r < 0$ . The parameters are taken to be  $\beta = 2$  and  $l = 3$ , the time range being  $0 < t < 0.001$  before the mainshock.

#### H. Spatial correlation of events after the mainshock

In this subsection, we examine the time-development of spatial correlations of events after the mainshock. The calculated spatial correlation functions are shown in Figs. 14 for the cases of  $\beta = 1$  (a), and of  $\beta = 2$  (b). As can be seen from the figures, after large events, small events remain active in a vicinity of the epicenter of the mainshock which may be regarded as aftershocks. Events are suppressed in the surrounding region where the displacement of the block was largest in the mainshock: See Fig. 3. Hence, it appears that the seismicity after the large event in the present model occurs so as to compensate the rupture in the mainshock. However, the seismicity near the epicenter is kept almost constant in time for some period after the mainshock, say, in the time range  $t < 0.03$ , which is in apparent contrast to the power-law decay as expected from the Omori law: See the insets of Figs. 14. At longer time scales, the seismicity near the epicenter exhibits the non-trivial time dependence as shown in the main panel of Figs. 14. In the case of  $\beta = 1$ , while the seismic activity near the epicenter seems to decay monotonically in this time range, the decay observed here is not a power-law decay as expected from the Omori-law. Hence, aftershocks obeying the Omori-law is not realized in the BK model, as already reported<sup>4</sup>. This is in apparent contrast to the observation for real faults.

Such an absence of aftershocks in the BK model might give a hint to the physical origin of aftershocks obeying the Omori-law, e.g., they may be driven by the slow chemical process at the fault, or by the elastoplasticity associated with the asenosphere, etc, which are not taken into account in the present model.

#### I. Time-dependent magnitude distribution

As another signature of the precursory phenomena, we show in Fig. 15 a "time-resolved" local magnitude distribution for several time periods before the large event, in the case of  $\beta = 1$  (Fig. 15(a)) and  $\beta = 2$  (Fig. 15(b)). Only the events with their epicenters within 30 blocks from the upcoming mainshock is counted here. As can be seen from the figures, as the mainshock approaches, the form of the magnitude distribution changes significantly. In particular, in the case of  $\beta = 1$ , the apparent  $B$ -value describing the power-law regime tends to increase as the mainshock approaches, from the time-averaged mean value  $\sim 0.50$  to the value  $\sim 1.0$  just before the mainshock: It is almost doubled. Interestingly,

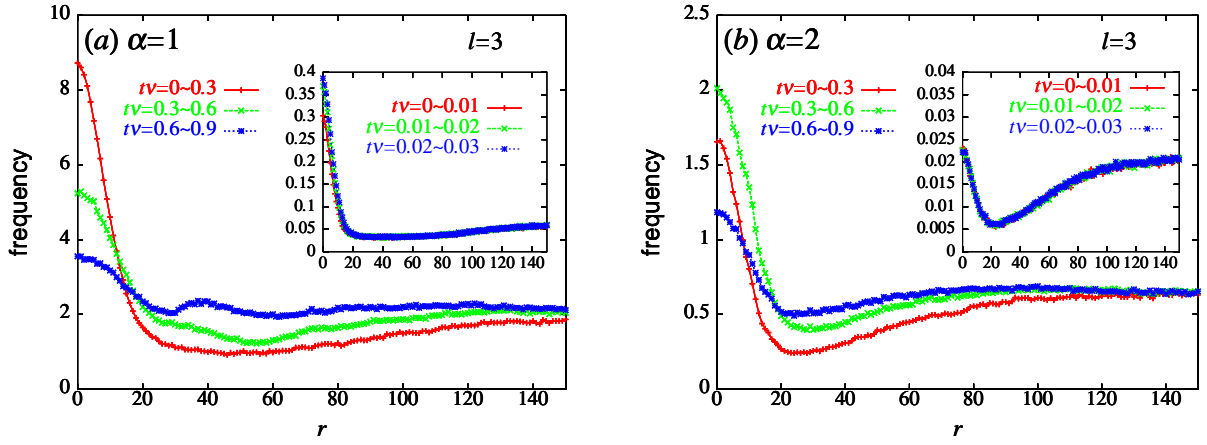


FIG. 14: Event frequency after the large event with  $\beta_c = 3$  plotted versus  $r$ , the distance from the epicenter of the upcoming mainshock, for several time periods after the mainshock. The parameter  $\alpha$  is 1 (a) and 2 (b), whereas  $l$  is fixed to  $l = 3$ . The main panel in each figure corresponds to the longer time scale, while the inset in each figure corresponds to the shorter time scale.

a similar increase of the apparent  $B$ -value preceding the mainshock was reported for real faults<sup>32</sup>. For the case of larger  $\beta_c = 2$  and 3, the change of the  $B$ -value preceding the mainshock is still appreciable, though in a less pronounced manner.

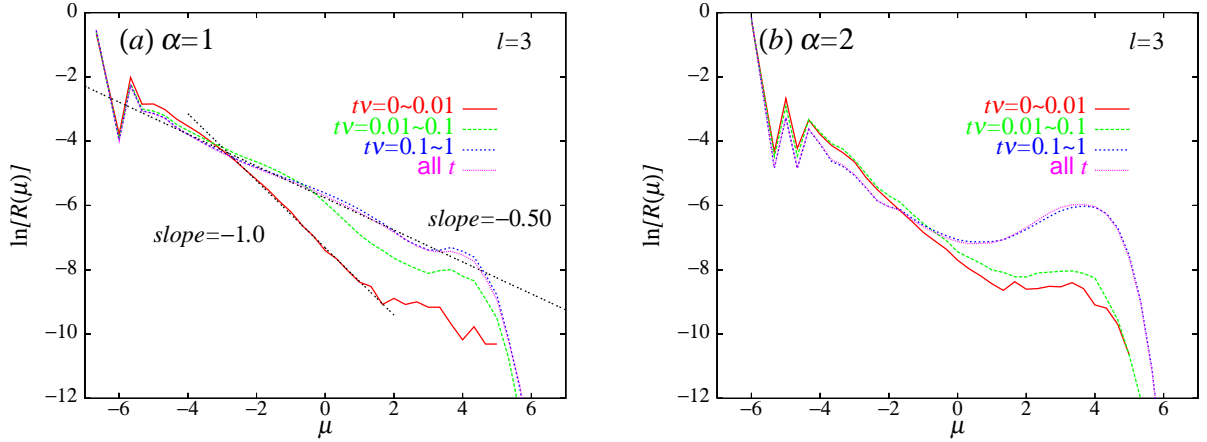


FIG. 15: Local magnitude distribution before the mainshock with  $\beta_c = 3$  for several time periods before the mainshock for the cases of  $\alpha = 1$  (a) and  $\alpha = 2$  (b).

In Fig.16, we show a similar time-resolved local magnitude distribution, but now after the large event, for the cases of  $\alpha = 1$  (Fig.16 (a)) and  $\alpha = 2$  (Fig.16 (b)). As can be seen from the figure, the form of the magnitude distribution changes only very little after the mainshock, in contrast to the one before the mainshock.

#### J. Time-predictable model versus size-predictable model

In describing the time sequence of earthquake events, two simplified models have widely been used, i.e., the size-predictable model and the time-predictable model<sup>2,33</sup>. These two models are considered to describe the two extreme situations of the earthquake occurrence.

In the size-predictable model, one assumes that the stress is released to some constant level just after the event, whereas the stress level at the onset of the rupture is random and unpredictable, as illustrated in Fig.17 (a). Within this scheme, when one can monitor the ongoing status of the stress, one can predict the size of an earthquake if it occurs at any given time, although the time of the next event is unpredictable.

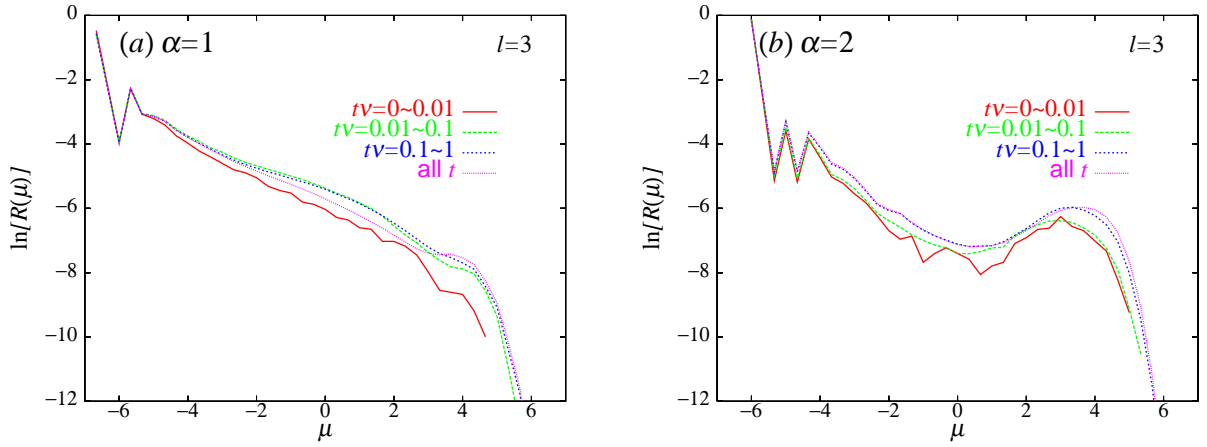


FIG .16: Local magnitude distribution after the mainshock with  $\alpha = 3$  for several time periods after the mainshock for the cases of  $\alpha = 1$  (a) and  $\alpha = 2$  (b).

In the time-predictable model, on the other hand, one assumes that an earthquake occurs whenever the accumulated stress reaches some constant level, whereas the size of the earthquake, i.e., the extent of the stress drop at the earthquake, is random and unpredictable, as illustrated in Fig.17 (b). One can predict within this scheme the time of the next event, though the size of the event is unpredictable.

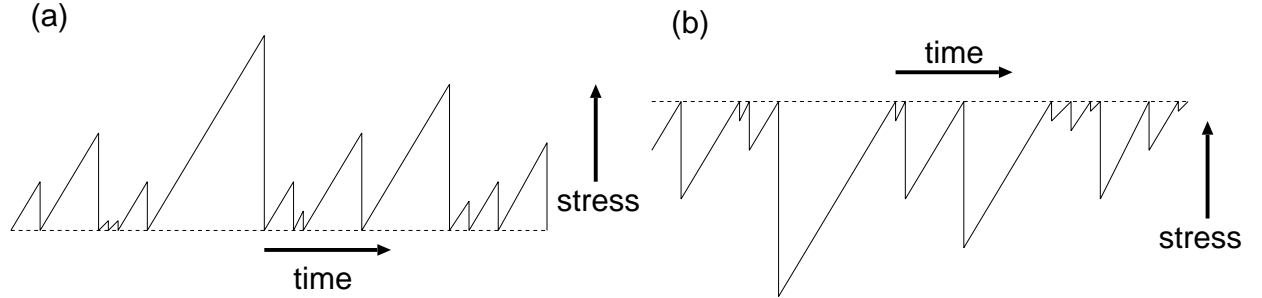


FIG .17: The size-predictable model (a) versus the time-predictable model (b).

In this subsection, we examine whether the time sequence of large events (with  $\alpha = 3$ ) of the present model is describable either by the time-predictable model or by the size-predictable model. Concerning the magnitudes of the successive earthquake events, both models predict no correlation. Our analysis of Figs.8 and 9 above revealed that the  $\alpha = 1$  model yielded no correlation between the magnitudes of the two successive events, while the  $\alpha = 2$  models yielded an anti-correlation between the magnitudes of the two successive events. Hence, concerning the magnitude correlation of the successive events, the  $\alpha = 1$  model is consistent with either the time-predictable model or the size-predictable model, while the  $\alpha = 2$  models are consistent with neither of them.

In order to further examine the compatibility of the model with the size- and time-predictable models, we show in Fig.18 the magnitude distribution of large events with varying the elapsed time since the last large event (waiting time). When the size-predictable model applies, the next event tends to be larger as one waits longer till the next event, whereas, when the time-predictable model applies, there should be no correlation between the waiting time and the size of the next event. As can be seen from Fig.18, there is a clear tendency irrespective of the value of  $\alpha$  that the next event tends to be larger as the waiting time gets longer. This property is compatible with the size-predictable model, but is incompatible with the time-predictable model.

In Fig.19, we show the distribution of the waiting time defined above with varying the magnitude of the last large event. When the time-predictable model applies, the waiting time tends to get longer as the size of the last large event gets larger, whereas, when the size-predictable model applies, there should be no correlation between the size of the last large event and the waiting time. As can be seen from Fig.19, the  $\alpha = 1$  model exhibits no correlation between the waiting time and the size of the last event, which is consistent with the size-predictable model, whereas

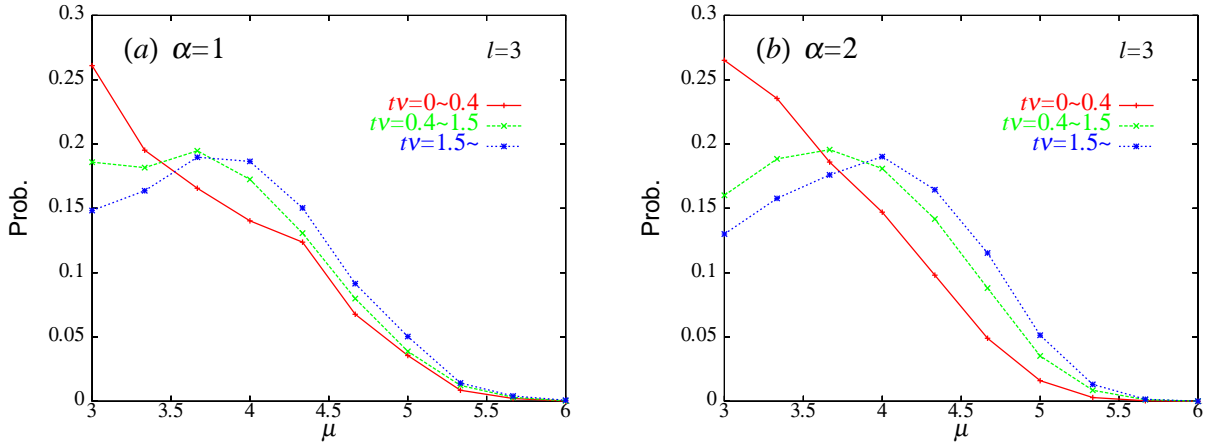


FIG . 18: The magnitude distribution of large events with  $\mu_c = 3$  for various values of the waiting time, i.e., the time elapsed since the last large event with  $\mu_c = 3$  which occurred within 30 blocks from the epicenter of the event. The parameter  $\alpha$  is  $\alpha = 1$  (a) and  $\alpha = 2$  (b), whereas the parameter  $l$  is fixed to be  $l = 3$ .

the  $\alpha = 2$  models exhibit a positive correlation between the waiting time and the size of the last event, which is apparently consistent with the time-predictable model.

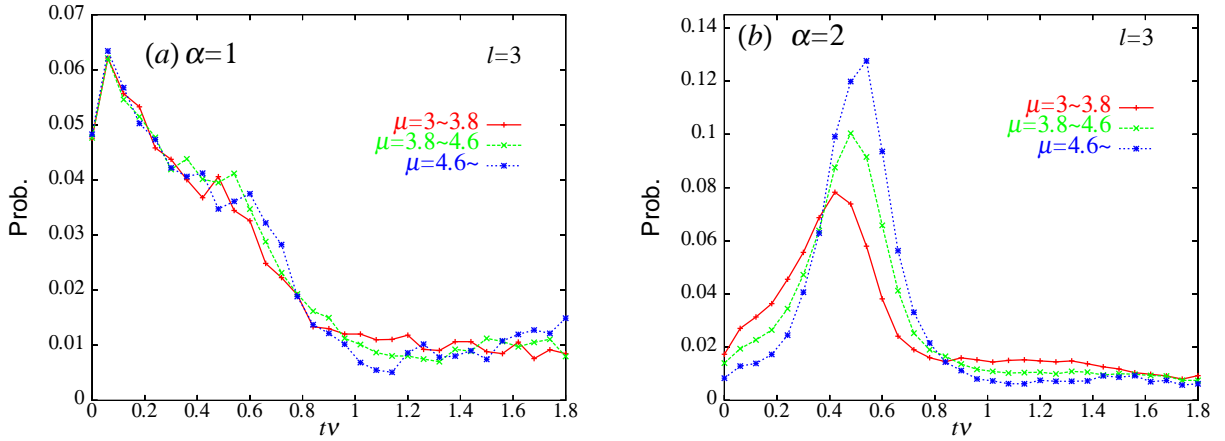


FIG . 19: The distribution of the waiting time, i.e., the time elapsed since the last large event with  $\mu_c = 3$  which occurred within 30 blocks from the epicenter of that event, for various values of the magnitude of the last large event. The parameter  $\alpha$  is  $\alpha = 1$  (a) and  $\alpha = 2$  (b), whereas the parameter  $l$  is fixed to be  $l = 3$ .

In view of all these observations, one may conclude that the  $\alpha = 1$  BK model is well describable by the size-predictable model, whereas the  $\alpha = 2; 3$  BK models are describable by neither the time-predictable nor the size-predictable model.

#### IV . S U M M A R Y A N D D I S C U S S I O N

In summary, we studied the spatio-temporal correlations of the 1D BK model of earthquakes with main focus on how the statistical properties of earthquakes depend on the frictional and elastic properties of earthquake faults. We have found that when the extent of the velocity-weakening property gets smaller, the system tends to be more critical, while, as the velocity-weakening property is enhanced, the system tends to be more  $\alpha$ -critical with enhanced features of characteristic earthquakes. Periodic feature of large events is eminent when the friction force exhibits a strong frictional instability, whereas when the friction force exhibits a weak frictional instability large events often occur as twin and/or unilateral events. The model with weaker frictional instability, i.e., the  $\alpha = 1$  model, is

well describable by the size-predictable model, while the model with stronger frictional instability, i.e., the 2 models, are describable neither by the size-predictable model nor the time-predictable model. We also observed several intriguing precursory phenomena associated with large events. Preceding the mainshock, the frequency of smaller events is gradually enhanced, whereas just before the mainshock it is suppressed only in a close vicinity of the epicenter of the upcoming mainshock (the Mogi doughnut). On the other hand, the Omori law of aftershocks is not observed in the present model. When the friction force exhibits a weak frictional instability, the apparent  $B$ -value of the magnitude distribution increases significantly preceding the mainshock.

Finally, it would be interesting to try some "real-world" prediction of various time and length scales associated with the seismic activity on the basis of the present results, e.g., the time and the length scales of the onset of the doughnut-like quiescence. For this purpose, we need to estimate the units of time and length of our model in terms of real-world earthquakes. Concerning our time unit  $t^1$ , we estimate it via the rise time of large earthquakes,  $t^1 = t^*$ , which is typically about 10 seconds. This gives an estimate of  $t^1 = 3 \text{ sec}^1$ . Concerning the length unit  $L$ , we estimate it making use of the fact that the typical displacement in large events of our simulation is of order one  $L$  unit, which in real-world large earthquakes is typically 5 meters. Then, we get  $L = 5 \text{ meters}$ . Since the loading rate  $\dot{u}^0$  associated with the real plate motion is typically 5 cm/year, the dimensionless loading rate  $\dot{u} = N(L \dot{u}^0)$  is estimated to be  $10^9$ . If we remember that the typical mean recurrence time of large events in our simulation is about one unit of  $t^1$ , the mean recurrence time of our simulation corresponds to 100 years in real world.

In our simulation, the doughnut-like quiescence was observed before the mainshock at the time scale of, say,  $t < 10^2$ . This time scale corresponds to about 1 year. In our simulation, the doughnut-like quiescence was observed in the region only within a few blocks from the epicenter of the mainshock. To give the corresponding real-world estimate, we need the real-world estimate of our block size  $a$ . In the present model, the length scale  $a$  is entirely independent of the length scale  $L$ , and has to be determined independently. We estimate  $a$  via the typical velocity of the rupture propagation,  $la^1$ , which is about 10 km/sec in real earthquakes. From this relation, we get  $a = 10 \text{ km}$ . If we remember that the rupture size of large events in our simulation with  $\dot{u} = \dot{u}_c = 3$  was about 60 blocks, the size of the rupture size of large earthquakes of our simulation corresponds to 600 km and more. The length scale associated with the doughnut-like quiescence is then estimated to be 20–30 km in radius.

Of course, earthquake is a complex phenomenon, and it is not a trivial matter at all how faithfully the statistical properties as observed here for the 1D BK model represent those of real earthquakes. After all, the BK model is a highly simplified statistical model where many features of real fault system have been neglected or simplified. Still, the model is expected to serve as a useful reference in identifying and elucidating the nature of real earthquakes. In particular, some of the precursory phenomena as observed here may have relevance to real earthquakes. We hope that the present study might give a step toward the fuller understanding of the statistical properties of earthquakes as a stick-slip dynamical instability.

---

<sup>1</sup> C.H. Scholz, Nature 391, 3411 (1998).

<sup>2</sup> C.H. Scholz, The Mechanics of Earthquakes and Faulting (Cambridge Univ. Press, 1990).

<sup>3</sup> R. Burridge and L. Knopoff, Bull. Seismol. Soc. Am. 57 (1967) 3411.

<sup>4</sup> J.M. Carlson and J.S. Langer, Phys. Rev. Lett. 62, 2632 (1989); Phys. Rev. A 40, 6470 (1989).

<sup>5</sup> J.M. Carlson, J.S. Langer, B.E. Shaw and C. Tang, Phys. Rev. A 44, 884 (1991).

<sup>6</sup> J.M. Carlson, J. Geophys. Res. 96, 4255 (1991).

<sup>7</sup> J.M. Carlson, Phys. Rev. A 44, 6226 (1991).

<sup>8</sup> J.M. Carlson, J.S. Langer and B.E. Shaw, Rev. Mod. Phys. 66, 657 (1994).

<sup>9</sup> J. Schmittbuhl, J.-P. Vilotte and S. Roux, J. Geophys. Res. 101, 27741 (1996).

<sup>10</sup> B.E. Shaw, J.M. Carlson and J.S. Langer, J. Geophys. Res. 97, 479 (1992).

<sup>11</sup> B.E. Shaw, Geophys. Res. Lett. 21, 1983 (1994).

<sup>12</sup> C.R. Myers and J.S. Langer, Phys. Rev. E 47, 3048 (1993).

<sup>13</sup> R. De and G. Ananthakrishna, Europhys. Lett. 66, 715 (2004).

<sup>14</sup> P. Bak, C. Tang and K. Wiesenfeld, Phys. Rev. Lett. 59, 381 (1987).

<sup>15</sup> P. Bak and C. Tang, J. Geophys. Res. 94, 15635 (1989).

<sup>16</sup> H. Nakanishi, Phys. Rev. A 41, 7086 (1990).

<sup>17</sup> K. Ito and M. Matsuzaki, J. Geophys. Res. 95, 6853 (1990).

<sup>18</sup> S.R. Brown, C.H. Scholz and J.B. Rundle, Geophys. Res. Lett. 18, 215 (1991).

<sup>19</sup> Z. Olan, H. J. Feder and K. Christensen, Phys. Rev. Lett. 68, 1244 (1992).

<sup>20</sup> A. Helmstetter, S. Hergarten and D. Sornette, Phys. Rev. Lett. 88, 238501 (2002); Phys. Rev. E 70, 046120 (2004).

<sup>21</sup> S. Hergarten and H. Neugebauer, Phys. Rev. E 61, 2382 (2000).

<sup>22</sup> S. Hainzl, G. Zoller and J. Kurths, J. Geophys. Res. 104, 7243 (1999); Geophys. Res. Lett. 27, 597 (2000).

<sup>23</sup> T. Mori and H. Kawamura, Phys. Rev. Lett. 94, 058501 (2005).

- <sup>24</sup> K. M. Ogi, Bull. Earthquake Res. Inst. Univ. Tokyo 47, 395 (1969); Pure Appl. Geophys. 117, 1172 (1979).
- <sup>25</sup> B. E. Shaw, J. Geophys. Res. 100, 18239 (1995).
- <sup>26</sup> C. R. Myers, B. E. Shaw and J. S. Langer, Phys. Rev. Lett. 77, 972 (1996).
- <sup>27</sup> J. Dietrich, J. Geophys. Res. 84, 2161 (1979).
- <sup>28</sup> A. Ruina, J. Geophys. Res. 88, 10359 (1983).
- <sup>29</sup> A. Corral, Phys. Rev. Lett. 92, 108501 (2004).
- <sup>30</sup> S. P. Nishenko and R. Buland, Bull. Seismol. Soc. Am. 77, 1382 (1987).
- <sup>31</sup> P. Bak, K. Christensen, L. Danon and T. Scanlon, Phys. Rev. Lett. 88, 178501 (2002).
- <sup>32</sup> W. D. Smith, Nature 289, 136 (1981).
- <sup>33</sup> K. Shimazaki and T. Nakata, Geophys. Res. Lett. 7, 279 (1980).